JACS
JOURNAL OF THE AMERICAN CHEMICAL SOCIETY

Subscriber access provided by American Chemical Society

Article

Recognition of RNA by Amide Modified Backbone Nucleic Acids: Molecular Dynamics Simulations of DNA–RNA Hybrids in Aqueous Solution

Mafalda Nina, Raymonde Fonn-Pfister, Renaud Beaudegnies, Habiba Chekatt, Pierre M. J. Jung, Fiona Murphy-Kessabi, Alain De Mesmaeker, and Sebastian Wendeborn

J. Am. Chem. Soc., **2005**, 127 (16), 6027-6038• DOI: 10.1021/ja0486566 • Publication Date (Web): 31 March 2005

Downloaded from http://pubs.acs.org on March 25, 2009

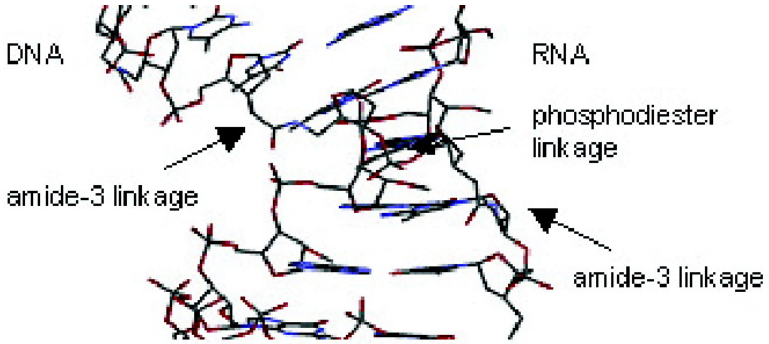

More About This Article

Additional resources and features associated with this article are available within the HTML version:

- Supporting Information
- Links to the 4 articles that cite this article, as of the time of this article download
- Access to high resolution figures
- Links to articles and content related to this article
- Copyright permission to reproduce figures and/or text from this article

View the Full Text HTML

ACS Publications
High quality. High impact.

Journal of the American Chemical Society is published by the American Chemical Society. 1155 Sixteenth Street N.W., Washington, DC 20036

J|A|C|S
ARTICLES
Published on Web 03/31/2005

Recognition of RNA by Amide Modified Backbone Nucleic Acids: Molecular Dynamics Simulations of DNA−RNA Hybrids in Aqueous Solution

Mafalda Nina,* Raymonde Fonné-Pfister, Renaud Beaudegnies, Habiba Chekatt, Pierre M. J. Jung, Fiona Murphy-Kessabi, Alain De Mesmaeker, and Sebastian Wendeborn

Contribution from the Syngenta Crop Protection AG, P.O. Box, CH-4002 Basel, Switzerland

Received March 9, 2004; Revised Manuscript Received February 16, 2005

Abstract: Thermodynamic and structural properties of a chemically modified DNA−RNA hybrid in which a phosphodiester linkage is replaced by a neutral amide-3 linkage (3′-CH_2-CONH-5′) were investigated using UV melting experiments, molecular dynamics simulations in explicit water, and continuum solvent models. van't Hoff analysis of the experimental UV melting curves suggests that the significant increase of the thermodynamic stability of a 15-mer DNA−RNA with seven alternated amide-3 modifications (+11 °C) is mainly due to an increased binding enthalpy. To further evaluate the origin in the observed affinities differences, the electrostatic contribution to the binding free energy was calculated by solving the Poisson−Boltzmann equation numerically. The nonelectrostatic contribution was estimated as the product of a hydrophobic surface tension coefficient and the surface area that is buried upon double strand formation. Structures were taken from 10 ns molecular dynamics simulations computed in a consistent fashion using explicit solvent, counterions, and the particle-mesh Ewald procedure. The present preliminary thermodynamic study suggests that the favorable binding free energy of the amide-3 DNA single strand to the complementary RNA is equally driven by electrostatic and nonpolar contributions to the binding compared to their natural analogues. In addition, molecular dynamics simulations in explicit water were performed on an amide-3 DNA single strand and the corresponding natural DNA. Results from the conformations cluster analysis of the simulated amide-3 DNA single strand ensembles suggest that the 25% of the population sampled within 10 ns has a pre-organized conformation where the sugar C3′ endo pucker is favored at the 3′-flanking nucleotides. These structural and thermodynamic features contribute to the understanding of the observed increased affinities of the amide-3 DNA−RNA hybrids at the microscopic level.

Introduction

During the past two decades, widespread interest in antisense therapeutics has led to the design of structurally diverse oligodeoxynucleotides which possess increased thermodynamic and biochemical properties. The heterocyclic bases, the deoxyribose sugar, and the phosphodiester linkage of the DNA strand have each undergone chemical modifications.[1] Phosphorothioates,[2] 2′-*O*-alkyl[1,3] and 2′-*O*-[2-(amino)-2-oxoethyl] nucleotides,[4] 2′-F-arabinoside substitutions,[5] cyclohexenyl sugar replacement,[6] and base alkyl substitutions such as a C5-methyl on pyrimidines[7−9] or unsaturated propyne groups[10] highlight some of the more recent modifications. While significant information has been collected about the chemical types of modifications that lead to improve duplex formation, little is known about the structural basis for the enhanced affinities. In general, RNA−RNA duplexes are more stable than corresponding DNA−DNA and DNA−RNA duplexes though the melting temperatures vary greatly with sequence.[7,11] The increased stability of RNA duplexes has been attributed to several structural features among which the most notable is the improved base stacking interactions that result from an A-form geometry.[12] The presence of a 2′-hydroxyl group in RNA largely accounts for the quite different conformations of DNA and RNA duplexes in solution by biasing the sugar toward a C3′ endo pucker (*N*-type), which results in the duplex preferably adopting the A-form geometry. Oligodeoxynucleotides prefer a C2′ endo sugar pucker (*S*-type), which is thought to impart a less stable B-form geometry.[13] A correlation between the electronegativity of the

* Corresponding author. E-mail: mafalda.nina@syngenta.com.

(1) Freier, S. M.; Altmann, K.-H. *Nucleic Acids Res.* **1997**, *25*, 4429−4443.
(2) Kanaori, K.; Tamura, Y.; Wada, T.; Nishi, M.; Kanehara, H.; Morii, T.; Tajima, K.; Makino, K. *Biochemistry* **1999**, *38*, 16058−16066.
(3) Lamond, A. I.; Sproat, B. S. *FEBS Lett.* **1993**, *325*, 123−127.
(4) Prakash, P. T.; Kawasaki, A. M.; Lesnik, E. A.; Owens, S. R.; Manoharan, M. *Org. Lett.* **2003**, *5*, 403−406.
(5) Trempe, J. F.; Wilds, C. J.; Denisov, A. Y.; Pon, R. T.; Damha, M. J.; Gehring, K. *J. Am. Chem. Soc.* **2001**, *123*, 4896−4903.
(6) Wang, J.; Verbeure, B.; Luyten, I.; Lescrinier, E.; Froeyen, M.; Hendrix, C.; Rosemeyer, H.; Seela, F.; Van Aerschot, A.; Herdewijn, P. *J. Am. Chem. Soc.* **2000**, *122*, 8595−8602.
(7) Lesnick, E. A.; Freier, S. M. *Biochemistry* **1995**, *34*, 10807−10815.
(8) Ono, A.; Ueda, T. *Nucleic Acids Res.* **1987**, *15*, 219−232.
(9) Walker, G. T. *Nucleic Acids Res*. **1988**, *16*, 3091−3099.
(10) Gyi, J. I.; Gao, D.; Conn, G. L.; Trent, J. O.; Brown, T.; Lane, A. N. *Nucleic Acids Res.* **2003**, *31*, 2683−2693.
(11) Conte, M. R.; Conn, G. L.; Brown, T.; Lane, A. N. *Nucleic Acids Res.* **1997**, *25*, 2627−2634.
(12) Searle, M. S.; Williams, D. H. *Nucleic Acids Res.* **1993**, *21*, 2051−2056
(13) Wang, S.; Kool, E. T. *Biochemistry* **1995**, *34*, 4125−4132.

substituent at 2′-position of the sugar and the conformation of the sugar pucker have been observed, suggesting that the amount of C3′ endo conformer increases linearly with the electronegativity of the 2′-substituent.[13] Moreover, the influence of the 2′-*O*-methylation due to conjunction of both electronegative 2′-substitution and steric effects stabilizes the sugar residues in their high C3′ endo conformation in a RNA.RNA duplex and DNA−RNA hybrids.[14,15] Methylation of the 2′-OH group shows that it has a negligible effect on the conformation of RNA duplexes.[16] In addition, the RNA duplex is further stabilized by a network of hydrogen bonds between water and the C2′-hydroxyl groups.[17] DNA−RNA duplexes are usually less stable than RNA.RNA duplexes and, depending on their sequences, more or less stable than DNA duplexes.[18,19] The structure of a hybrid duplex is intermediate between the A- and B-form geometries, which may result in poor stacking interactions. The stability of a DNA−RNA hybrid is central to antisense therapies, as the mechanism requires binding of a modified DNA to an mRNA thereby selectively inhibiting the synthesis of the target protein. To effectively inhibit the mRNA transcription, the antisense DNA should have a very high binding affinity for the complementary mRNA. Furthermore, the modified DNA−RNA hybrid structure should be unperturbed relative to the unmodified DNA−RNA duplex in order to invoke RnaseH recognition and thereby induce subsequent degradation of the RNA strand. Generally, it appears that oligodeoxynucleotides favoring *N*-type sugar conformation display an increased helical thermostability relative to the native DNA, when hybridized with complementary RNAs. Although structures of nucleic acids that favor *N*-type conformation nucleotides have been determined, little is known about their features underlying increase in their thermostability.

In the present work we were interested in chemically modified oligonucleotides in which the natural phosphodiester linkage found in DNA is substituted by amide linked units producing chimeric molecules that bind to RNA targets with greater stability compared to their wild-type DNA counterpart. [20−22] In particular, amide-3 modified backbone nucleic acids are analogues of DNA in which the natural phosphodiester linkage found in the physiological nucleic acids are replaced with an uncharged "peptide-like" backbone (Figure 1).

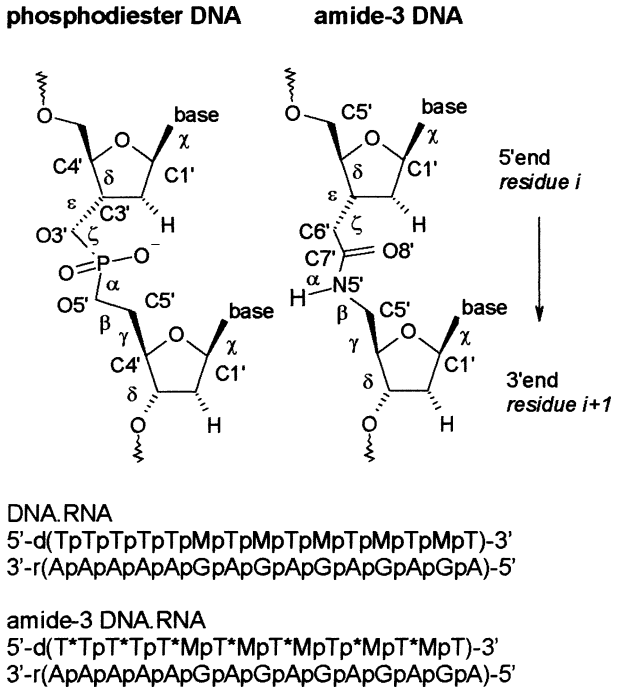

Figure 1. Natural phosphodiester linkage and the amide-3 linkage proposed as a substitute for the phosphodiester in antisense oligonucleotides. The modified strand has two types of residues: residue *i*, in which the amide-3 linkage is attached to C3′, and residue $i + 1$, in which the amide-3 linkage is attached at C5′. * denotes the amide-3 linkage, p denotes the phosphodiester linkage, and M denotes the 5-methylcytosine.

It has been demonstrated that one DNA strand with one such amide-3 modified backbone linkage can recognize a RNA single strand and forms a duplex which mimics the behavior of the natural DNA−RNA hybrid. The replacement of a phosphodiester linkage in 2′-deoxyoligonucleotides by an amide bond provides a +0.4 °C increase in thermal stability per modification, compared to an unmodified DNA oligonucleotide control of the same sequence and length hybridized with a 2′-OH RNA strand.[20] The higher binding affinity has been partially attributed to the absence of a gauche effect between the oxygen atoms of −O−C4′−C3′−O3′− of the native phosphodiester linkage, causing a C3′ endo sugar pucker of residue *i*, which in turn may give the oligomer a favorable A-form like geometry (Figure 1).[23] Moreover, it has been suggested that the amide-3 backbone exists in a conformation pre-organized for the binding to the complementary RNA. To understand the relative binding affinity and specificity of the amide-3 modified DNA for the RNA target, it is important to understand their structure, dynamics, relative flexibility, binding free energies and hydration pattern compared to the natural DNA−RNA duplex. Theoretical calculations, particularly molecular dynamics (MD) simulations have proven to be powerful techniques for the structural study of modified[21,24,25] and unmodified duplexes,[26−29] triplexes, and

(14) Auffinger P.; Westhof E. *Angew. Chem. Int. Ed. Engl.* **2001**, *40*, 4648−4650.
(15) Kawai, G.; Yamamoto, Y.; Kamimura, T.; Masegi, T.; Sekine, M.; Hata, T.; Iimori, T.; Watanabe, T.; Miyazawa, T.; Yokoyama, S. *Biochemistry* **1992**, *31*, 1040−1046.
(16) Popenda M.; Biala, E.; Milecki, J.; Adamiak, R. W. *Nucleic Acids Res.* **1997**, *25*, 4589−4598.
(17) Egli, M.; Portmann, S.; Usman, N. *Biochemistry* **1996**, *35*, 8489−8494.
(18) Saenger, W. *Principles of Nucleic Acid Structure*; Springer-Verlag: New York, 1984.
(19) Matveeva, O. V.; Tsodikov, A. D.; Giddings, M.; Freier, S. M.; Wyatt, J. R.; Spiridonov, A. N.; Shabalina, S. A.; Gesteland, R. F.; Atkins, J. F. *Nucleic Acids Res.* **2000**, *28*, 2862−2865.
(20) (a) Lebreton, J.; De Mesmaeker, A.; Waldner, A.; Fritsch, V.; Wolf, R. M. Freier, S. M. *Tetrahedron Lett.* **1993**, *34*, 6383−6386. (b) De Mesmaeker, A.; Waldner, A.; Lebreton, J.; Hoffmann, P.; Fritsch, V.; Wolf, R. M.; Freier, S. M. *Angew. Chem. Ed. Engl. Engl.* **1994**, *34*, 226−229. (c) De Mesmaeker, A.; Waldner, A.; Fritsch, V.; Lebreton, J.; Wolf, R. M. *Bull. Soc. Chim. Belg.* **1994**, *103*, 705−715. (d) De Mesmaeker, A.; Wendeborn, S.; Jouanno, C.; Fritsch, V.; Wolf, R. M. *Bioorg. Med. Chem.* **1997**, *7*, 1869−1874. (e) De Mesmaeker, A.; Jouanno, C.; Wolf, R. M.; Wendeborn, S. *Bioorg. Med. Chem.* **1997**, *7*, 447−452. (f) De Mesmaeker, A., Lebreton, J.; Jouanno, C.; Fritsch, V.; Wolf, R. M.; Wendeborn, S. *Synlett* **1997**, *11*, 1287−1290.
(21) (a) Fritsch, V.; De Mesmaeker, A.; Waldner, A.; Lebreton, J.; Blommers, M. J. J.; Wolf, R. M. *Bioorg. Med. Chem.* **1995**, *3*, 321−335. (b) Wolf, R. M.; De Mesmaeker, A.; Waldner, A.; Wendeborn, S.; Fritsch, V.; Lebreton, J. *New J. Chem.* **1997**, *21*, 61−72.
(22) Wilds, C. J.; Minasov, G.; Natt, F.; Von Matt, P.; Altmann, K.-H.; Egli, M. *Nucleosides Nucleotides Nucleic Acids*, **2001**, *20*, 991−994.
(23) Blommers, M. J. J.; Pieles, U.; De Mesmaeker, A. *Nucleic Acids Res.* **1994**, *22*, 4187−4194.
(24) Sen, S.; Nilsson, L. *J. Am. Chem. Soc.* **2001**, *123*, 7414−7422.
(25) Venkateswarlu, D.; Lind, K. E.; Mohan, V.; Manoharan, M.; Ferguson, D. M. *Nucleic Acids Res.* **1999**, *27*, 2189−2195.
(26) MacKerell, A. D., Jr.; Nilsson, L. *Computational Biochemistry and Biophysics*; Marcel Dekker: New York, 2001; p 441−463.
(27) Damm, W.; Frontera A.; Tirado-Rives J.; Jorgensen W. L. *J. Comput. Chem.* **1997**, *18*, 1955−1970.
(28) Nina, M.; Simonson, T. *J. Phys. Chem. B* **2002**, *106*, 3696−3705.

other forms of nucleic acids.[30−33] Previous MD simulations of a 14-mer DNA with seven alternated amide-3 backbone linkages hybridized with the complementary 2′-OH RNA performed with the AMBER force field where electrostatic interactions were modeled with a distance-dependent dielectric constant thus lacking detailed interatomic interactions with water molecules and counterions. The latter study reported that the modified sequences might assume different conformations that allow for standard Watson−Crick base pairing with a complementary RNA strand without major strain or steric hindrance.[21] To complement these earlier studies and to examine the effect of the inclusion of explicit water, counterions and a different long-range electrostatic treatment, we report here four independent MD simulations of 10 ns each in which DNA, RNA, counterions, and solvent are treated in atomic detail and the long-range electrostatic interactions are treated by particle-mesh Ewald summation under periodic boundary conditions. Moreover an estimate of the differences in binding free energies of the natural and amide-3 modified DNA−RNA hybrids was investigated by combining the explicit molecular dynamics simulations with continuum solvation models based on previous approaches.[34]

In this paper, we report the relative thermal stability of duplexes formed by a natural 15-mer DNA strand and a modified 15-mer DNA strand with seven alternated amide-3 linkages hybridized with complementary 2′-*O*-Me RNA fragments. We have carried out systematic studies of molecular dynamic simulations of (i) a 15-mer DNA−RNA duplex with seven alternated amide-3 backbone modifications, (ii) a 15-mer native DNA−RNA hybrid of the same sequence, (iii) a 15-mer DNA single strand with seven amide-3 alternated backbone modifications, and (iv) a 15-mer native DNA single strand and have compared their structural, dynamic and solvation properties in water. For the native and modified DNA−RNA hybrids, the starting conformation was set as a canonical A-form. For each single strand, the starting conformation was helicoidal with all of the bases stacked sequentially on the top of each other. The electrostatic contribution to the binding free energies was computed using both a finite-difference Poisson−Boltzmann model, and the nonelectrostatic contributions to the binding free energies were estimated with a solvent accessible surface area dependent term. For the energetic analysis, structures were taken as snapshots from nanosecond length molecular dynamics simulations computed in a consistent fashion in explicit solvent, applying the particle mesh Ewald method and the CHARMm force field. The results provide a picture of the flexibility of both duplexes and single strands in explicit water on the nanosecond time scale and a physical interpretation for the origins of the relative stabilities of the natural DNA−RNA and the amide-3 modified backbone DNA−RNA hybrids. They also allow us to gain insight into the induced changes in nucleic acid structures due to the amide-3 backbone modifications, which might be important for understanding the features underlying the improved binding characteristics of this chemically modified oligonucleotide to complementary RNA.

Materials and Methods

(i) Experimental Section. *Synthesis of the Amide-3 Oligonucleotides.* Amide-3 backbone modified building blocks were synthesized according to a reported procedure.[35] Corresponding phosphoramidites were efficiently incorporated into oligonucleotides using solid-phase synthesis.[36] Oligonucleotides were synthesized on an Expedite Model 8909 Nucleic Acid Synthesis System using 1 μmol scale. The standard protocol was modified in the detritylation cycle. The oligomers were cleaved from the support and unprotected by treating the controlled pore glass support with concentrated ammonia overnight. Molecular weights were determined by mass spectroscopy. Unprotected oligomers were synthesized DMT-on and were purified by preparative C-18 reverse phase HPLC. The separation method allowed simultaneous purification, desalting and removal of the DMT.

UV Melting Experiments and Thermodynamical Profiles of Duplexe Formation. Unmodified DNA and 2′-*O*-Me RNA were obtained from Eurogentec. Thermal denaturation profiles were measured with a Cary 300 Bio spectrophotometer with the use of quartz microcuvettes of 1 cm optical length. The temperature of the cell holder containing the cuvettes was heated at 90 °C for 15 min and decreased from 90 to 0 °C with a rate of 0.5 °C/min. The absorbance at 260 nm was measured every 0.5 min from 75 to 105 °C and half-dissociation evaluation was performed. Concentrations of the unmodified DNA−RNA duplex and the amide-3 modified backbone DNA−RNA duplex were 1.38 and 1.02 μM respectively in a buffer with 10 mM NaCl, 10 mM potassium phosphate, at pH 6.0. The concentration of the DNA single strands was determined using the extinction coefficient of 117.6 $M^{-1}cm^{-1}$ for the nonmodified strand and was 112.1 M^{-1} cm^{-1} for the amide-3 DNA strand. The 2′-*O*-Me RNA single-strand concentration was determined using the extinction coefficient of 191.2 M^{-1} cm^{-1}. The midpoint of this absorption versus temperature profile is defined as the melting point (T_m), reflecting the temperature at which equal fractions of oligonucleotides are paired and single stranded under equilibrium. The UV melting curves were analyzed to obtain van't Hoff transition enthalpies.[37] The analysis required converting the experimental absorbance versus temperature into a melted fraction α versus temperature curve. This conversion is accomplished graphically by taking the ratio at each temperature of the height between the upper baseline and the experimental curve and the height between the lower and upper baselines.[37]

(ii) Molecular Dynamics Simulations. *Initial Structures.* One sequence of native DNA d(T1pT2pT3pT4pT5pM6pT7pM8pT9pM10pT11 pM12pT13pM14pT15) and one modified DNA with seven alternated amide-3 backbone linkages d(T1*T2pT3*T4pT5*M6pT7*M8pT9*M10pT11*M12pT13*M14pT15) complemented with a 2′-*O*-Me RNA single strand were considered in this study where p stands for the natural phosphodiester linkage, * stands for the amide-3 linkage and M stands for 5-methylcytosine. Two additional single DNA strands with identical sequences and lengths i.e d(T1pT2pT3pT4pT5pM6pT7pM8pT9pM10pT11 pM12pT13pM14pT15) and d(T1*T2pT3*T4pT5*M6pT7*M8pT9*M10pT11*M12pT13*M14pT15) were also considered. Cytosines were replaced with 5-methylcytosines in the oligodeoxynucleotides since they increase the DNA−RNA hybrid binding energy due to beneficial hydrophobic interactions of the C(5)-methyl groups in the duplex structures.[8,9,10] The choice of polypyrimidine sequences was motivated by the simplified building block synthesis of pT*T and pT*M dimers. The choice of using 2′-*O*-Me substituted RNA

(29) Cheatham, T. E., III.; Kollman, P. A. *J. Mol. Biol.* **1996**, *259*, 434−444.
(30) Feig, M.; Zacharias, M.; Pettitt, B. M. *Biophys. J.* **2001**, *81*, 352−370.
(31) Spackova, N.; Berger, I.; Sponer, J. *J. Am. Chem. Soc.* **2001**, *123*, 3295−3307.
(32) Beveridge, D. L.; McConnel, K. J. *Curr. Opin. Struct. Biol.* **2000**, *10*, 182−196.
(33) Norberg, J.; Nilsson, L. *Acc. Chem. Res.* **2002**, *35*, 465−472.
(34) Kollman, P. A.; Massova, I.; Reyes, C.; Kuhn, B.; Huo, S.; Chong, L.; Lee, M.; Lee, T.; Duan, Y.; Wang, W.; Donini, O.; Cieplak, P.; Srinivasan, J.; Case, D. A.; and Cheatham, III, T. E. *Acc. Chem. Res.* **2000**, *33*, 889−897.
(35) De Mesmaeker, A.; Lesueur, C.; Bévierre, M.-O.; Waldner, A.; Fritsch, V.; Wolf, R. M. *Angew. Chem. Ed. Engl. Engl.* **1996**, *35*, 2790−2794.
(36) For synthesis of nucleotides see ref 14 in De Mesmaeker A.; Lebreton, J.; Hoffmann, P.; Freier, S. M. *Synlett.* **1993**, *9*, 677−697.
(37) Marky, L. A.; Breslauer, K. J. *Biopolymers* **1987**, *26*, 1601−1620.

was dictated by the greater resistance of the corresponding nucleotides to nuclease[38] and also by an easier solid-phase synthesis compared to the natural RNA.[23] No experimental structures of the 15-mer DNA−RNA oligonucleotides considered in the present work have been successfully obtained so far. Consequently, one starting structure was considered for each system and was built with the settings of the Biopolymer module of InsightII (Accelrys, San Diego) with standard A-type parameters and all sugars in the *N*-type conformation.

Setup of Solvated Systems. Each oligomer was neutralized with ammonium counterions according to the number of charged phosphate groups. The counterions were initially placed at positions of low electrostatic potential. The electrostatic potential due to the oligomers was calculated at the positions of the water oxygen atoms by solving the Poisson equation as implemented in the Delphi module of InsightII assuming dielectric constants of $\epsilon = 1$ inside the oligomers and $\epsilon = 80$ outside. The water oxygen atom position with the lowest potential was replaced by a counterion. The electrostatic potential calculation was then repeated including the first counterion. This process was repeated until the number of counterions necessary to neutralize the structure was positioned. Each structure was immersed in a periodic orthorhombic box of TIP3 water molecules of $47 \times 47 \times 92$ Å.[39] Water molecules that were closer than 2.8 Å from any atom of the solute molecule or counterion were deleted. Each unit cell includes the DNA−RNA hybrid or the DNA single strand, NH_4^+ counterions and about 6,500 water molecules for a total of about 20,500 atoms.

MD Simulation Methodology. All MD simulations reported in this work were performed using the CHARMm module of InsightII (Accelrys, San Diego) and the CHARMM27 force field for nucleic acids.[40,41] Force field parameters for the amide-3 backbone modification were abstracted directly whenever possible from the all-atom CHARMM nucleic acids and proteins sets.[40−42] Existing CHARMM atom types were assigned to the "peptide-like" backbone atoms (see Supporting Information Figure 1). The charges on the additional C2′-OCH_3 groups replacing the C2′-OH groups of the RNA strands (+0.1) were set to maintain the neutral overall charge balance in the sugar consistent with the CHARMM27 force field for nucleic acids. Parameters for ammonium were adapted from the OPLS force field of Jorgensen[43] and from the methylammonium parameters from CHARMM25 and tested by solvation free energy calculations.[28] All simulations were performed in the isothermic isobaric ensemble ($T = 300$ K, $P = 1$ atm). Long-range interactions were treated using the particle-mesh Ewald (PME) method.[44] The PME charge grid spacing was 1 Å and the charge grid was interpolated using the cubic B-spline (order 4) at the 8 Å direct space cutoff. Constant temperature and pressure was maintained throughout the simulations using the Hoover algorithm. A time step of 0.002 ps was used to integrate the equation of motion with a nonbonded pairlist update frequency of 0.020 ps. All bonds involving hydrogen atoms were constrained with the SHAKE algorithm.[45] Before beginning the production run, the following thermalization and equilibration protocols were applied. First, the water molecules and the counterions in the periodic box and the lattice parameters were energy-minimized with the oligonucleotides fixed, followed by 50 ps of MD simulation at 300 K, i.e., thermalization. Second, the whole system, including the solute, counterions and water molecules, was subjected to 500 steps of energy minimization to remove close contacts. Last, positional restraints were added to the oligonucleotides atoms and gradually reduced over 50 ps of MD at 300 K. Unrestrained simulations of the unmodified DNA−RNA hybrid, the amide-3 modified DNA−RNA hybrid, the unmodified DNA single strand, and the amide-3 modified single strand were continued for 10 ns each. The coordinates were written every 0.001 ps and stored for subsequent analysis. The resulting trajectories were analyzed using the CHARMm module of InsightII. The standard helicoidal parameters were deduced using the FREEHELIX98 program.[46] All calculations were performed on a Silicon Graphics Origin2000 fitted with 8 SGI/R10000 processors using the MPI version of CHARMm program. Each simulation demanded approximately 90 s of CPU time per psec of simulation time on one processor.

(iii) Cluster Conformations Analysis. The cluster analysis was performed for the natural and amide-3 modified backbone single strands using a method derived from a previous work.[47] For each simulation, 2500 structures were extracted from the last 5 ns of the trajectory at 0.002 ps intervals for analysis. The clustering was performed in Cartesian space. For each structure, a least-squares translational and rotational fit was performed with the heavy atoms of residues 4−11 and the atom positional root-mean-square difference (RMSd) for this set of atoms was calculated. Terminal residues were not taken into account, as they tend to have more freedom of motion. The number of structures satisfying the similarity criterion set to RMSd ≤ 3 Å for the heavy atoms was determined in the pool of 2500 structures. The structure with the highest number of neighbors (i.e., structures satisfying the similarity criterion) was taken as the central member of the first cluster. All structures belonging to the first cluster were removed from the pool. The number of neighbors was computed again with the remaining structures. The structure with the highest number of neighbors becomes the central member of the second cluster. The process is iterated until all structures were assigned to a cluster. A detailed description of the clustering method can be found elsewhere.[47]

(iv) Binding Free Energies Analysis of Natural and Amide-3 Modified DNA−RNA Hybrids. The total free energy can be estimated from the molecular mechanical energy, the solvation free energy, and the vibrational, rotational, and translational entropies for the DNA, following previously developed methods.[48−50] Solute entropies contribution to the free energies is one of the most difficult terms to estimate in this model. Solute entropies have been estimated by different methods (harmonic and quasiharmonic approximations) and indicated to be dependent on the number of snapshots used and the portion of trajectory analyzed. Since the principal difference between the natural DNA−RNA and the amide-3 modified backbone lies in the phosphate-phosphate repulsions, which are greater in the natural DNA−RNA hybrid as 15-mer amide-3 DNA−RNA has five neutral linkages replacing five phosphodiester linkages, we investigated the binding free energies difference of both double strands. Consequently, the binding free energy was approximated based on the assumption that the amide-3 DNA, natural DNA, and the complementary RNA conformations are the same in the double strand and in the dissociated form thus neglecting the rotational, translational and vibrational entropy contributions. The binding free energy (ΔG^{bind}) between the two complementary strands is calculated as the sum of the Coulomb and van der Waals DNA-RNA interaction energies and the difference

(38) Uhlmann E.; Peyman, A. *Chem. Rev.* **1990**, *90*, 544−579.
(39) Jorgensen, W.; Chandrasekar, J.; Madura, J.; Irnpey, R.; Kelin, M. *J. Phys. Chem.* **1983**, *79*, 926−935.
(40) Foloppe, N.; MacKerell, Jr., A. D. *J. Comput. Chem.* **2000**, *21*, 86−104.
(41) MacKerell, A. D.; Banavali N. *J. Comput. Chem.* **2000**, *21*, 105−120.
(42) MacKerell, A.-D.; Bashford, D.; Bellott, M.; Dunbrack, R. L.; Evanseck, J. D.; Field, M. J., Fischer, S.; Gao, J.; Guo, H.; Ha, S.; Joseph-McCarthy, D.; Kuchnir, L.; Kuczera, K.; Lau, F. T. K.; Mattos, C., Michnick, S.; Ngo, T.; Nguyen, D. T.; Prodhom, B.; W. E.-Reiher, III, Roux, B.; Schlenkrich, M.; Smith, J. C.; Stote, R.; Straub, J.; Watanabe, M.; Wiorkiewicz-Kuczera, J.; Yin, D.; Karplus, M. *J. Phys. Chem. B* **1998**, *102*, 3586−3616.
(43) Jorgensen, W. L.; Chandrasekhar, J.; Madura, J. D.; Impey, R. W.; Klein, M. *J. Chem. Phys.* **1983**, *79*, 926−935.
(44) Feller, S. E.; Pastor, E. W.; Rojnuckarin, A.; Bogusz, S.; Brooks, B. R. *J. Phys. Chem.* **1996**, *100*, 17011−17020.
(45) Ryckaert, J. P.; Ciccotti, G.; Berendsen, J. C. *J. Comput. Chem.* **1977**, *23*, 327−341.
(46) Dickerson, R. *Nucleic Acids Res.* **1998**, *26*, 1906−1926.
(47) Hamprecht, Fred A.; Peter, Christine; Daura, Xavier; Thiel, Walter; van Gunsteren, Wilfred F. *J. Chem. Phys.* **2001**, *114*, 2079−2089.
(48) Srinivasan, J., Cheatham, T. E., Cieplak, P., Kollman, P. A.; Case, D. A. *J. Am. Chem. Soc.* **1998**, *120*, 9401−9409.
(49) Jayaram, B.; Sprous, D.; Young, M. A.; Beveridge, D. L. *J. Am. Chem. Soc.* **1998**, 120: 10629−10633.
(50) Cheatham, T. E., Srinivasan, J., Case, D. A.; Kollman, P. A. *J. Biomol. Struct. Dyn.* **1998**, *16*, 265−280.

between the solvation free energies of the double strands and the dissociated system:

$$\Delta G^{\text{binding}} = E^{\text{Coul}}{}_{(\text{DNA}-\text{RNA})} + E^{\text{vdW}}{}_{(\text{DNA}-\text{RNA})} + \Delta G^{\text{solv}}{}_{(\text{double strand})} - \Delta G^{\text{solv}}{}_{(\text{DNA})} - \Delta G^{\text{solv}}{}_{(\text{RNA})}$$

where the subscript "DNA-RNA" refers to the intramolecular DNA−RNA interaction energy terms, and the subscripts "double strand", "DNA" and "RNA" refer to the solvation free energies of the double strand, DNA single strand and RNA single strand, respectively. We applied the same force field and parameter set used in the MD simulations to compute the Coulomb energy (E^{Coul}) and the van der Waals energy (E^{vdW}) but without cutoff for nonbonded interactions.

The solvation free energy (ΔG^{solv}) was estimated from the electrostatic solvation energy (ΔG^{PB}) and the nonpolar solvation energy ($\Delta G^{\text{nonpolar}}$):

$$\Delta G^{\text{solv}} = \Delta G^{\text{PB}} + \Delta G^{\text{nonpolar}}$$

The electrostatic contribution to the solvation free energy (ΔG^{PB}) was calculated using the nonlinear Poisson−Boltzmann method[51−53] and using the UHBD program.[54] This method approximates the electrostatic solvation free energy (ΔG^{PB}) as the reaction field energy of removing a solute from vacuum to water.[55] An external dielectric of 80 was used to simulate the aqueous environment, while the interior of the oligonucleotides was simulated by a dielectric constant of 1, 2, and 4. Different solute dielectric constants were used in order to evaluate which value better captures the electronic response of the macromolecule.[56] We employed a physiological 150 mM salt concentration to calculate salt effect on the solvation free energies.[57] Atomic charges for natural and amide-3 modified backbone DNA and RNA are the same as those used in the molecular mechanical energy calculations.[40−42] We applied the van der Waals radii parameter set for atomic radii as in CHARMM27 force field,[40−42] and used a probe radius of 1.4 Å to define the dielectric boundary. The radii for hydrogen atoms are set to zero, and a reentrant surface was used for the dielectric boundary. For the UHBD calculations a grid spacing of 0.5 grid/Å, in which the longest linear dimension of the solute occupied 80% of the lattice was used. The boundary potential was calculated using the Debye−Huckel approximation for half number of the boundary points. The boundary potential of the rest was interpolated from the nearest grid points. A total of 300 linear iterations followed by 2000 nonlinear iterations were performed for each snapshot to reach convergence, as further judged by the root-mean-square deviation (RMSD) between successive iterated potential maps being less than 10^{-5}.

The nonpolar contribution to the solvation free energy (G_{nonpolar}) was estimated as

$$\Delta G^{\text{nonpolar}} = \gamma S_{\text{A}} + b,$$

where $\gamma = 0.00542$ kcal/A^2, $b = 0.86$ kcal/mol, and S_{A} is the solvent accessible surface area.[58] The water-accessible surface area S_{A} was calculated by rolling a 1.4 Å probe on the protein van der Waals surface while atomic radii were taken from the set of van der Waals atomic radii.[40−42] Snapshots from the MD trajectories of the natural and amide-3 modified backbone DNA−RNA hybrids with water and counterions removed were considered for the binding free energy calculations. A total of 1000 snapshots were selected at 2 ps intervals from each of the last 2 ns trajectory.

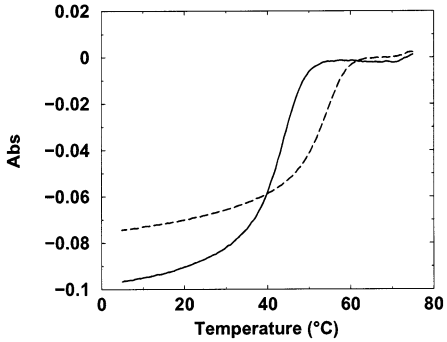

Figure 2. UV melting profiles (260 nm) obtained for the unmodified DNA−RNA (solid line) and the amide-3 modified backbone DNA−RNA (dashed line). The melting temperatures (T_{m}) are 43.6 °C ± 0.7 and 54.2 °C ± 0.6, respectively.

Table 1. Thermodynamic Stability of DNA−RNA Hybrids: Effect of Amide-3 Modifications at 298K[a]

DNA–RNA	ΔG_{vH}	ΔH_{vH}	$T\Delta S_{\text{vH}}$	T_{m}
amide-3	−17	−93	−76	53.4 (0.6)
natural	−14	−87	−73	41.9 (0.7)
D	−3	−6	−3	+11.5

[a] Δ is defined as (amide-3 DNA−RNA) − (natural DNA−RNA). Energy values are in kcal/mol.

Results

UV Absorbance Melting Curves. The helix-to-coil transition of antiparallel amide-3 DNA−RNA and unmodified DNA−RNA hybrids were characterized by UV melting curves monitored by the absorbance value at 260 nm. The two curves follow the characteristic sigmoidal behavior for the unfolding of a nucleic acid duplex as shown in Figure 2. Reproducible melting curves were obtained for each type of duplex. The melting temperature, T_{m}, was obtained from the maximum of the first derivative of the absorbance with respect to the absolute temperature. The measured thermal stability of the two duplexes shows that the modified DNA−RNA duplex with seven alternated amide-3 modifications in the DNA strand complemented with a 2′-*O*-Me RNA strand is more stable ($T_{\text{m}} = 54.2$ °C ± 0.6) compared to the natural DNA−RNA ($T_{\text{m}} = 43.6$ °C ± 0.7) by about 11 °C.

Thus, the amide-3 backbone modifications in the DNA strand results in ΔT_{m} per modification of about 1.5 °C, where ΔT_{m} is the difference between the melting temperature of the amide-3 modified and unmodified DNA−RNA hybrids. van't Hoff analysis[37] was used to determine the transition enthalpies ΔH_{vH} for the helix-coil transition of each duplex from the shape of the melting curves. van't Hoff plots of melted fraction α versus temperature were constructed for the two duplexes from the UV absorbance melting curves (see Supporting Information Figure 2).

The underlying assumption when applying this graphical evaluation of the thermodynamic parameters is that the DNA melting transition occurs in a two-state manner. These graphically evaluated thermodynamic parameters are summarized in Table 1. van't Hoff enthalpies and extrapolated ΔG values determined from the UV melting studies on the duplexes indicated that the increased thermodynamic stability of the

(51) Warwicker, J.; Watson H. C. *J. Mol. Biol.* **1982**, *157*, 671−679.
(52) Sharp, K. A.; Honig, B. *J. Phys. Chem.* **1990**, *94*, 7684−7692.
(53) Sharp, K. A.; Honig B. *Annu. Rev. Biophys. Biophys. Chem.* **1990**, *19*, 301−332.
(54) Davis M. E.; Madura J. D.; Luty, B. A.; MacCammon. J. A. *J. Comput. Chem.* **1991**, *12*, 909−912.
(55) Honig, B.; Nicholls, A. *Science.* **1995**, *268*, 1144−1149.
(56) Sham, Y. Y.; Chu, Z. T. Warshel, A. *J. Phys. Chem. B* **1997**, *101*, 4458−4472.
(57) Sharp, K. A.; Honig, B. *Curr. Opin. Struct. Biol.* **1995**, *5*, 323−328.
(58) Sitkoff, D.; Ben-Tal, N.; Honig, B. *J. Phys. Chem.* **1996**, *100*, 2744−2752.check

Table 2. Average RMS Difference (Å)[a]

	heavy	base	sugar	Phos	amide-3
Versus Averaged Structure					
amide-3	1.4 (0.4)	1.1 (0.3)	1.4 (0.4)	1.8 (0.5)	1.4 (0.4)
natural	1.4 (0.3)	1.0 (0.2)	1.3 (0.3)	1.7 (0.4)	–
Versus A Form					
amide-3	2.0 (0.5)	1.5 (0.4)	2.1 (0.5)	2.5 (0.5)	1.8 (0.4)
natural	1.7 (0.3)	1.3 (0.3)	1.6 (0.3)	2.1 (0.4)	–

[a] Averages over the final 4 ns were included. RMS fluctuations are in parentheses.

amide-3 DNA−RNA is due to an increased binding enthalpy as compared to the unmodified DNA−RNA hybrid.

DNA−RNA Modified and Unmodified Duplexes. *(a) Analysis of the MD Trajectories.* All trajectories started from the A-type conformation. These simulations were extended to 10 ns to ensure that the last 4 ns of the trajectories were properly converged for the analysis. Average root-mean-square differences (RMSd) and RMS fluctuations (RMSf) for the amide-3 and natural DNA−RNA hybrids simulations are presented in Table 2. In both cases the averaged conformations and the canonical A conformations are used as reference states. Table 2 reveals differences between the amide-3 and natural DNA−RNA hybrids with respect to the reference structures.

The RMSd of both natural and amide-3 DNA−RNA hybrids are smaller when the reference state was the averaged structure versus the canonical A form. In addition the natural DNA−RNA hybrid is closer with respect to the canonical A form compared to the amide-3 DNA−RNA hybrid with RMSd of 1.7 and 2.0 Å, respectively, for all heavy atoms. The RMSd of the bases and phosphates from the natural and amide-3 modified DNA−RNA hybrids simulations with respect to the MD-averaged structure were similar with the differences between those moieties being of 0.7 Å, while the amide-3 backbone RMSd with respect to the MD-averaged form were of 1.4 Å with the amide-3 backbone variations, less than the phosphates (1.8 Å). This observation indicates that the structural properties of the amide-3 backbone differ in modified DNA−RNA versus the natural hybrid DNA−RNA with a phosphodiester backbone.

Calculations of the root-mean-square fluctuations (RMSf) from their MD-averaged structures give an estimate of the differences in local flexibility due to chemical differences of the backbone (Table 2). The RMS fluctuations for the bases, sugars and phosphate groups are similar for the natural and modified DNA−RNA with slightly large fluctuations for the individual moieties in the modified DNA−RNA hybrid (by 0.1 Å). Differences in the RMSf between the individual moieties in both oligonucleotides indicate that the motions of the bases, phosphate and sugars are relatively independent.

(b) Structures Analysis. Average Structures. Average structures of the unmodified and amide-3 DNA−RNA hybrids were calculated over the last 4 ns of the trajectories (Figure 3). The two structures are almost homomorphous with geometries close to the A-type. Helicoidal parameters describe the relative orientation of bases with respect to either a global helical axis or locally adjacent base pairs.[59,60] Table 3 reports selected helicoidal parameters and corresponding standard deviations from the MD-averaged structures of the amide-3 DNA−RNA,

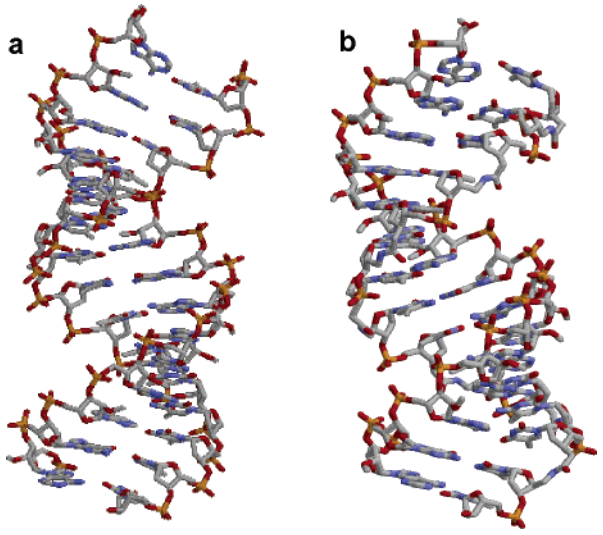

Figure 3. Average structures over the last 4 ns of (a) the unmodified DNA−RNA hybrid and (b) the amide-3 modified DNA−RNA. The two structures are homomorphous with A-type geometries. The RMSd between the amide-3 and the unmodified DNA−RNA MD-averaged structures and the A-form initial structures are 2.0 and 1.7 Å respectively. Overall, the hybrid duplexes have a similar minor groove despite the introduction of amide-3 linkages in the amide-3 DNA−RNA duplex. The amide-3 carbonyl group (C7′(O8′) in Figure 1) is pointing toward the major groove.

the unmodified DNA−RNA, and NDB (Nucleic acids Databank) reported DNA−RNA for polypyrimidine−polypurine structures.[61−63] The MD simulations satisfactorily reproduce a variety of helicoidal parameters of the hybrid polypyrimidine−polypurine structures.

Base Stacking. Analysis of the unmodified and amide-3 DNA−RNA MD-averaged structures shows that the structures sampled during the dynamics correspond to an A-form double helix (see Figure 3) with global twist angles in the range of 31.9 ± 2.1° and 34.8 ± 3.1° respectively. The number of residues per turn for the unmodified and amide-3 DNA−RNA hybrids is 5.8 and 5.4 respectively indicating that the amide-3 alternated backbone modifications lead to a slightly underwound structure compared to the natural one. The twist angle changes dramatically along the sequences of both unmodified and modified DNA−RNA duplexes as shown in Figure 4. The TpT and CpT steps have an average twist value of about 32° when excluding the two residues at the 5′- and 3′-ends. A lower twist value is observed at the C6pT7 step of the natural DNA−RNA duplex (average about 28°).

Higher twist values are observed for the CpT steps of the amide-3 modified DNA−RNA duplex (average about 36°) compared to the natural DNA−RNA duplex. Interestingly, the twist values between the amide-3 steps are similar to the twist values between two corresponding consecutive base pairs in the natural DNA−RNA, indicating that the amide-3 backbone modification induces a change in the twist of the steps below and above but not in the step connected by the amide-3 linkage itself. Overall, the introduction of amide-3 modifications slightly decreases the stacking between consecutive bases as reflected by a slight increase in the global twist angle found for the averaged amide-3 DNA−RNA as compared to the unmodified DNA−RNA hybrid.

(59) Dickerson, R. *J. Biomol. Struct. Dynam.* **1989**, *6*, 627−634.
(60) Hartmann, B.; Lavery, R. *Q. Rev. Biophys.* **1996**, *29*, 309−368.
(61) Xiong, Y.; Sundaralingam, M. *Nucleic Acids Res.* **2000**, *28*, 2171−2176.
(62) Conn, G., Brown, T., Leonard, G. *Nucleic Acids Res.* **1999**, *27*, 555−561.

Table 3. Relative Orientation of Bases with Respect to Global Helical Axis or Locally Adjacent Base Pairs[a]

	rise	incl	roll	twist	X-disp	slide
			MD Simulation			
amide-3	2.6 (0.8)	8.3 (18.0)	7.4 (3.7)	34.8 (3.1)	−1.3 (3.0)	−2.2 (0.1)
natural	2.9 (0.1)	16.0 (7.0)	7.0 (3.6)	31.9 (2.1)	−4.6 (0.5)	0.004 (0.06)
			NBD Survey			
DNA.RNA[b]	3.4	14.0	8.1	31.2	−4.0	1.5
DNA.RNA[c]	3.3	10.4	5.4	29.1	−4.6	1.7
DNA.RNA[d]	3.1	8.0	4.2	30.6	−4.2	1.8

[a] All parameters were calculated for the 7 central base pairs T_5*M_6pT_7*M_8pT_9*M_{10}pT_{11} over the last 4 ns with FREEHELIX98.[46] NBD structures are from DNA−RNA hybrids with purine-rich and pyrimidine-rich strands for comparison with the present work. [b] Crystal structure of the hybrid d(CTCTTCTTC).r(GAAGAAGAG).[61] [c] Crystal structure of the hybrid d(GCTTCTCTTC). r(GAAGAGAAGC).[62] [d] 10 NMR structures of r(GAAGAGAAGC).d(GCTTCTCTTC).[63] Averaged values as in NDB databank base.

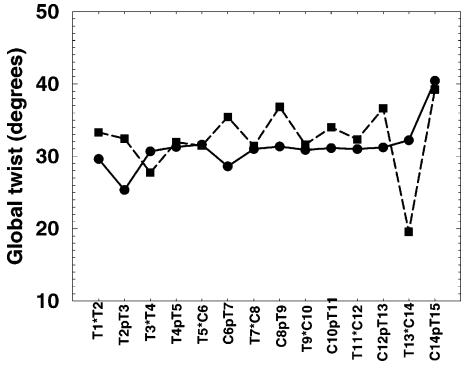

Figure 4. Global twist along the sequence from 5′-end to 3′-end for the MD-averaged structures of the unmodified (solid line) and amide-3 (dashed line) DNA−RNA duplexes. * indicates a dimer connected either by an amide-3 linkage or by a phosphodiester linkage, p indicates a dimer connected by a phosphodiester linkage.

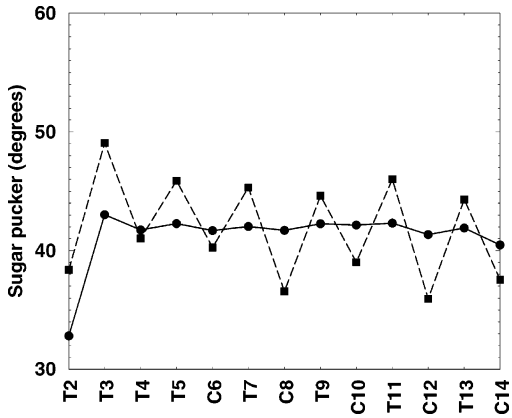

Figure 5. Amplitude pseudorotation angles along the DNA sequence from 5′-end to 3′-end for the MD-averaged structures of the unmodified (solid line) and amide-3 (dashed line) of the DNA−RNA duplexes. 5′- and 3′-end residues are not shown.

Backbone Conformational Flexibility. To gain deeper insight into the relative flexibility of the hybrid duplexes, we compared the amide-3 DNA and unmodified DNA dihedral angles sampled during the MD simulations. Most backbone angles for the DNA strand in the unmodified DNA−RNA reside in the normal ranges for right-handed duplex structures as proposed for the solution structures of DNA−RNA hybrids with all-pyrimidine and all-purine strands.[63,64] Two different conformations were found which can be distinguished by their α (O3′−P−O5′−C5′), β (P−O5′−C5′−C4′) and γ (O5′−C5′−C4′−C3′) backbone angles (Figure 1). The preferred backbone conformation of the DNA strand of the unmodified DNA−RNA duplex is gauche-/trans/gauche+ as found in both canonical A- and B-DNA. We observed a spontaneous flipping of α, β and γ to trans/gauche+/trans, corresponding to that proposed for the experimental structure of poly dT.poly rA hybrids.[63−65] The α, β and γ backbone angles of the phosphodiester linkages of the amide-3 DNA strand are in a predominant gauche−/trans/gauche+ as found in the DNA of the unmodified DNA−RNA duplex, whereas ϵ and ζ-angles in the same linkages sampled each a unique range of values trans and gauche−, respectively, for both unmodified and modified duplexes. However, the ζ-angles of the modified DNA strand display a broad distribution near gauche− compared to the unmodified strand. Moreover, rare spontaneous flips of α, γ from gauche−/gauche+ to gauche+/trans were observed in the phosphodiester linkages. The amide-3 linkages are characterized by their α (C6′−C7′−N5′−C5′), β (C7′−N5′−C5′−C4′) and γ (N5′−C5′−C4′−C3′) backbone angles (Figure 1). The trans conformation of the α-angle is imposed in the amide-3 linkage. The γ backbone angles are found trans whereas β-angles display broad distributions near −120°. The preferred conformation of the amide-3 backbone is then trans−/−120°/trans. Spontaneous flipping of the β, ζ-angles from −120°, −120° to gauche+, gauche+ were observed during the simulation run. The β, ζ-angles also sampled another stable conformation trans/gauche+ correlated with a change in the sugar pucker from C3′ endo to C2′ endo. The broader distribution of the β, γ and ϵ backbone angle values found for the amide-3 DNA strand as compared to the unmodified DNA strand indicates an overall greater flexibility for the modified DNA within the corresponding duplexes. The α, β, ζ-angles of the predominant conformations of the 2′-*O*-Me RNA complementary strand of the unmodified and amide-3 DNA−RNA hybrids are gauche−/trans/gauche+ and the ϵ, ζ-angles −120°/gauche−, indicating that there are not significant changes in the ϵ, ζ backbone angles of the 2′-*O*-Me RNA regardless the complementary DNA strand nature.

Furanose Ring Puckers. The average sugar pucker amplitudes for the unmodified DNA−RNA duplex vary from 41° ± 5° to 43° ± 5° along the oligomer whereas the amide-3 DNA−RNA duplex amplitudes vary from 37° ± 5° to 49° ± 5° indicating that in both duplexes the sugar conformation samples the C3′ endo region toward C4′exo. Again, the sugar pucker values change dramatically along the sequence as shown in Figure 5. The sugar pucker amplitudes of the residues $i + 1$ (Figure 1) have a low average value of 38° compared to residues i (46°).

(63) Gyi, J. I.; Lane, A. N.; Conn, G. L.; Brown, T. *Biochemistry* **1998**, *37*, 73−80.
(64) Sanghani, S. R.; Lavery, R. *Nucleic Acids Res*. **1994**, *22*, 1444−1449.
(65) Zimmermann, S. B.; Pheiffer, B. H. *Proc. Natl. Acad. Sci. U.S.A.* **1981**, *78*, 78−92.

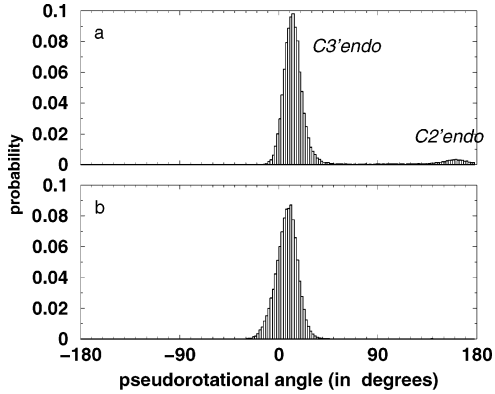

Figure 6. Histograms of the phase pseudorotation angles of (a) the natural and (b) the amide-3 DNA strands sampled along the duplexes 10 ns-MD simulations. The sugar puckers of the amide-3 DNA strand sample most exclusively the *C3′ endo* conformation whereas the sugar puckers of the natural DNA strand sample both *C3′ endo* and *C2′ endo* conformations.

Overall, the simulations data indicate that the amide-3 sugar puckers in the duplex are globally locked in the C3′ endo conformation whereas the natural DNA sugar puckers samples the C3′ endo and C2′ endo conformations as showed in Figure 6.

Residues *i* C8, C10, C12, and C14 sampled the C2′ exo conformation. In agreement with previous experimental results,[16,66] it is observed that the 2′-*O*-Me groups are locked into a single orientation (toward the minor groove), corresponding to one of the three orientations adopted by the 2′-OH groups in the unmodified RNA. The puckering amplitudes of the RNA complementary strands of the unmodified and amide-3 DNA are 43° ± 5 and 41° ± 5 respectively, indicating that there are not significant changes in the sugar conformation of the complementary RNA (C3′ endo region).

(c) Solvent and Counterions Structure. Water Molecules. The average water structure around the unmodified and amide-3 DNA−RNA duplexes is characterized here by the radial distribution function $g_i(r)$, which measures the probability of finding the oxygen atom of a solvent molecule at the distance r from a particular atom *j* of the duplex along the first 3 ns of each trajectory. The integrated value of $g_j(r)$ corresponds to the time-average, running coordination number of atom *j*. The radial distribution function (rdf) around a particular atom *j* gives information about the stability of the water site. rdfs and coordination numbers have been calculated for each of the seven C7′ atoms of the amide-3 modifications, and the phosphate atoms of the seven alternated phosphodiester linkages of the amide-3 DNA−RNA duplex. These rdfs were compared with the corresponding phosphate atom rdfs of the unmodified DNA−RNA duplex (see Supporting Information Figure 3). The solvation structure is remarkably similar for all phosphate groups regardless of the presence of the 3′- and 5′- flanking amide-3 modified linkages. The rdfs have a sharp peak at 2.9 Å from P atoms and a running coordination number of 1.5−2, indicating a structured site and a high degree of occupancy i.e., 1.5−2 water molecules on average for both duplexes. The rdfs of the carbon atom C7′ of the carbonyl group which reflects the hydration of the amide-3 group have broader peaks and a lower degree of occupancy with running coordination number of 1, indicating a single structured water at the amide-3 C7′(O8′) sites of the major groove.

(66) Lubini, P.; Zurcher, W.; Egli, M. *Chem. Biol.* **1994**, *1*, 39−45.

Table 4. Energies Contributions to the Free Energy of Binding of the Amide-3 Modified Backbone and Natural DNA−RNA Hybrids[a]

	amide-3 DNA–RNA	natural DNA–RNA
$\langle \Delta G_{\text{nonpolar(DNA−RNA)}} \rangle$	31 (0.2)	31 (0.3)
$\langle \Delta E^{\text{vdW}}{}_{\text{(DNA−RNA)}} \rangle$	−96 (10)	−87 (10)
$\langle \Delta E^{\text{Coul}}{}_{\text{(DNA−RNA)}} \rangle_{\epsilon=1}$	1955 (27)	3653 (49)
$\langle \Delta G_{\text{PB}} \rangle_{\epsilon=1}$	−1973 (37)	−3657 (59)
$\langle \Delta G_{\text{elec}}{}^{\text{binding}} \rangle_{\epsilon=1}$	−18 (7)	−5 (7)
$\langle \Delta E^{\text{Coul}}{}_{\text{(DNA−RNA)}} \rangle_{\epsilon=2}$	978 (13)	1826 (24)
$\langle \Delta G_{\text{PB}} \rangle_{\epsilon=2}$	−983 (19)	−1823 (28)
$\langle \Delta G_{\text{elec}}{}^{\text{binding}} \rangle_{\epsilon=2}$	−5 (4)	3 (4)
$\langle \Delta E^{\text{Coul}}{}_{\text{(DNA−RNA)}} \rangle_{\epsilon=4}$	489 (7)	914 (12)
$\langle \Delta G_{\text{PB}} \rangle_{\epsilon=4}$	−488 (8)	−906 (14)
$\langle \Delta G_{\text{elec}}{}^{\text{binding}} \rangle_{\epsilon=4}$	1 (3)	8 (3)

[a] All mean energies over 1000 structures are in kcal/mol. Values in parentheses are standard deviations of the mean energies. Δ is defined as (DNA−RNA) − (RNA.single strand + DNA single strand) binding energies. ⟨ ⟩ denotes an average over a set of snapshots along an MD trajectory. Ion concentration: 150 mM. $\langle \Delta G_{\text{PB}} \rangle = \Delta G^{\text{solv}}{}_{\text{(DNA−RNA)}} - \Delta G^{\text{solv}}{}_{\text{(DNA)}} - \Delta G^{\text{solv}}{}_{\text{(RNA)}}$. $\langle \Delta G_{\text{elec}}{}^{\text{binding}} \rangle$ stands for the electrostatic contribution to the binding energy: $\langle \Delta E^{\text{Coul}}{}_{\text{(DNA−RNA)}} \rangle + \langle \Delta G_{\text{PB}} \rangle$

Ammonium Counterions. The simulations also provided a detailed description of the counterion structure and dynamics. rdfs between the phosphorus atoms of the phosphodiester linkage and the carbon atoms of the amide-3 carbonyl groups and the nitrogen of the NH_4^+ indicate that when an ordered ammonium site occurs, the position of the first peak (near 3.8 Å) does not depend on the nature of the atom i.e., phosphorus or carbon of the amide-3. However, the ordered ion sites found for the unmodified DNA−RNA with the highest degree of occupancy (coordination number of 0.5) were found disordered in the amide-3 DNA−RNA simulation.

(d) Binding Free Energies of Amide-3 DNA−RNA and Natural DNA−RNA Hybrids. Further insight into the forces involved in duplex binding can be obtained by analyzing the binding free energy contributions, which are listed in Table 4 for the amide-3 and natural DNA−RNA hybrids. Comparing the van der Waals/nonpolar ($\Delta E^{\text{vdW}}{}_{\text{(DNA−RNA)}} + \Delta G_{\text{nonpolar}}$) with the electrostatic ($\Delta E^{\text{Coul}}{}_{\text{(DNA−RNA)}} + \Delta G_{\text{PB}}$) contributions, we find that the association between the amide-3 DNA and the complementary 2′-*O*-Me RNA, and between the natural DNA and the complementary 2′-*O*-Me RNA, is mainly driven by more favorable nonpolar interactions in the complex than in solution. This has been proposed as a general scheme for noncovalent association.[67] However, as indicated in the energy components of the amide-3 and natural DNA−RNA hybrids, this driving force is considerably weaker in the natural DNA−RNA as compared to the amide-3 modified DNA−RNA hybrid. The free energy penalty $\langle \Delta G_{\text{elec}}{}^{\text{binding}} \rangle$ is less for the natural DNA−RNA than for the amide-3 DNA−RNA hybrid and, together with their large van der Waals contribution consequently, leads to the highest binding affinity in the amide-3 DNA−RNA hybrid. Although we cannot compare the computed binding free energies for the modified and natural DNA−RNA hybrids with the enthalpies differences from UV melting experiments, the calculated value for binding of the amide-3 DNA−RNA hybrid is predicted to be more stable by 22 kcal.mol^{-1} compared to the natural DNA−RNA hybrid, and assuming that the dielectric constant of the solute is 1 and a ionic strength of 0.15 M. When a dielectric constant of 2 or 4 is assigned to the solute, the

(67) Miyamoto, S.; Kollman, P. A. *Proc. Natl. Acad. Sci. U.S.A.* **1993**, *90*, 8402−8406.

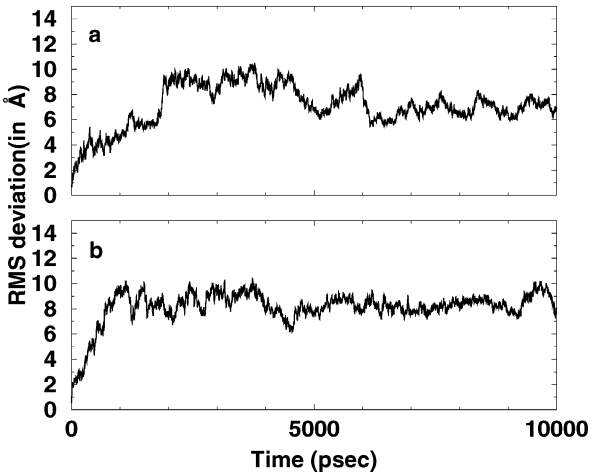

Figure 7. Time evolution of the rmsd from the unmodified (a) and amide-3 (b) DNA single strands. Initial structures are in the A-form.

calculated values for the binding of the amide-3 DNA−RNA hybrid are predicted to be more stable by 17 and 16 kcal.mol^{-1} respectively. Overall, the calculated main contributors to the enthalpy difference observed between the natural and modified DNA−RNA hybrids are found equally driven by nonpolar (about 9 kcal.mol^{-1} more favorable for the amide-3 DNA−RNA) and electrostatic (13, 8 or 7 kcal.mol^{-1} more favorable for the amide3-DNA−RNA if the solute dielectric constant is 1, 2 or 4 respectively) interactions between complementary strands (Table 4).

Modified and Unmodified DNA Single Strands. *(a) Analysis of the MD Trajectories.* The rmsd of the unmodified and amide-3 DNA single strands changed significantly with time, indicating that the structures deviated from the respective starting structures and thus spanned over a wide range of conformations during the 10 ns simulations (see Figure 7). The amide-3 DNA retains a more conserved A-form structure for the first 1 ns, stabilized for about 600 ps (average rmsd around 6 Å) than shows a sharply increased rmsd (9 Å) which then remains stable for the last 4 ns of the simulation (averaged rmsd around 7 Å). For the unmodified DNA single strand, the rmsd rises to 4 Å within the first 1000 ps and averages around 8 Å in the final stages of the simulation.

(b) Clustering Analysis of the Amide-3 and Natural DNA Single Strands Conformations. A conformational-clustering algorithm has been used to characterize the configurational space sampled in the simulations of the natural and amide-3 modified backbone simulations at 300K (see Materials and Methods). The number of clusters of conformations from these two trajectories was calculated as a function of time (not shown). The number of clusters is approximately constant over the last 5 ns of the two independent trajectories, but there is no definite indication of convergence, i.e., of complete sampling of configurational space. Nevertheless, the most relevant (probable) conformations (clusters), i.e., the conformations with lowest free energy, sampled within the last 5 ns period were considered here for analysis.

The number of conformations sampled is larger in the simulation of the natural DNA single strand (22 clusters) than in the simulation the amide-3 modified backbone DNA single strand (18 clusters). This is further illustrated in Figure 8, where the clusters from the trajectories are decomposed in terms of

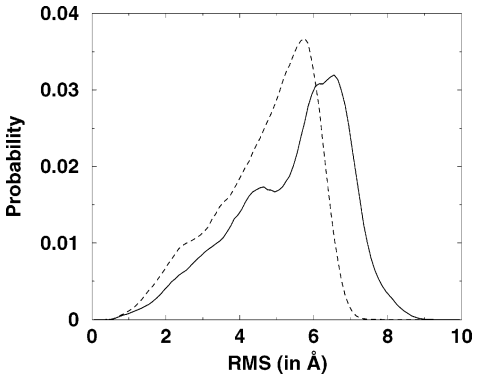

Figure 8. Percentages of members as a function of the similarity criterion, i.e., RMSd ≤ 3 Å. Natural DNA single strand in solid line, amide-3 modified backbone DNA single strand in dotted line.

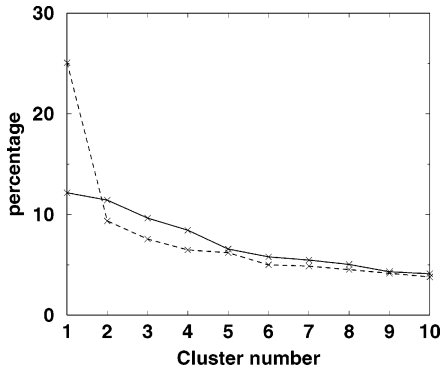

Figure 9. Percentage of members from the simulation in clusters 1−10 when the conformational clustering is performed over the last 5 ns correspond to the simulations of the natural and amide-3 DNA single strand. The crosses indicate the percentage of structures from the total of 2500 structures analyzed.

percentages of members as a function of the similarity criterion, i.e., rmsd. Results suggest that the natural DNA single strand conformations sampled a larger conformational space, i.e., broader rmsd distribution as compared to the amide-3 DNA single strand. Cluster analysis of the trajectory of the amide-3 modified backbone DNA single strand shows that the most stable conformation (first-ranked cluster; see Figure 10A) is adopted 25% of the time during the last 5 ns of the simulation as shown in the Figure 9. Such conformation is characterized by a C3′ endo sugar pucker phase for the bases T4 to T11 (except the base C10 which adopts a C2′ endo conformation). Moreover, the amide-3 DNA single strand samples ca. half of its time in the first 5 clusters (from the total of 18). Regarding the weight of the most populated clusters of the natural DNA single strand, cluster number 1 contains approximately 12% of the whole (2500) ensemble of structures, and the first 6 clusters (from the total of 22) contain as much as 50% of the ensemble. These numbers suggest that the most relevant parts of the conformational space accessible to the amide-3 modified backbone DNA single strand at 300 K have been already sampled within the 10 ns simulations, even if the complete space has not been sampled.

Although not representing significant clusters sampled during the trajectories, the conformational space accessible to the amide-3 modified backbone DNA single strand includes sampled conformations "hairpin-like". Two different "hairpin-like" structures forming a loop of four bases are observed at the 5′end of the single strand stabilized either by the stacking between the

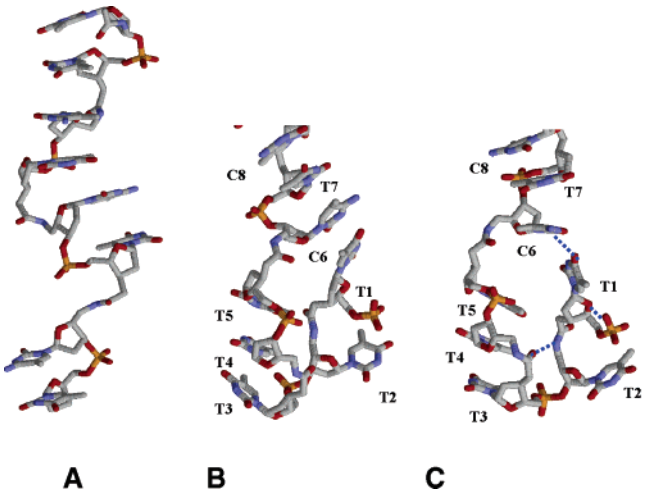

Figure 10. (A) The most relevant (probable) conformation (first-ranked cluster) is adopted 25% of the time during the last 5 ns of the simulation of the amide-3 modified backbone DNA single strand. Only the center of the cluster is showed for clarity. Most of the bases adopted a *C3′ endo* conformation. (B) Two conformations of the amide-3 DNA single strand rarely sampled during the 10 ns trajectory. The stacking interaction between the bases T1 and C6 stabilized the loop. The structures are colored according to the atom types. (C) The "hairpin-like" structure is stabilized by two hydrogen bonds: one between NH3 of the C6 base ring and the C(O) of T1 and the other between the amide-3 carbonyl linkage T3*T4 and the amide-3 NH group of the T1*T2 linkage.

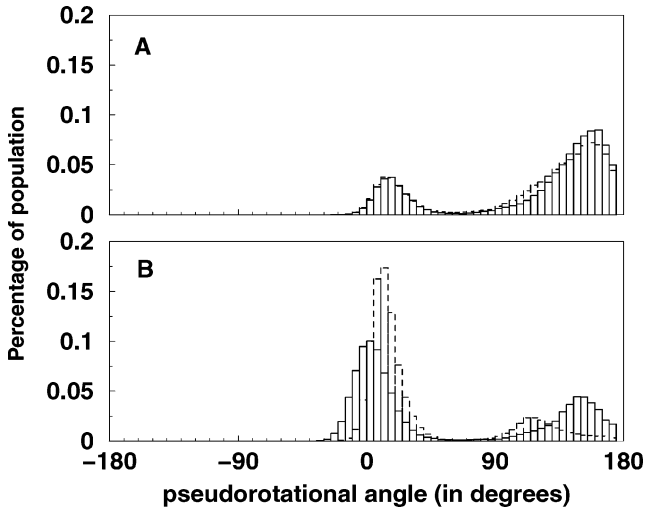

Figure 11. Phase pseudorotational profiles of the residues *i* (dashed line) and *i* + 1 (solid line) (as defined in Figure 1) (a) in the alternated amide-3 modified DNA single strand over a 10 ns simulation and (b) in the native DNA single strand.

bases T1 and C6 (Figure 10B) (with five consecutive bases i.e., T1, C6, T7, C8 and T9 remaining stacked) or by two intramolecular hydrogen bonds: one formed by the NH group of the amide-3 linkage between T1 and T2 with the C7′(O8′) group of the amide-3 linkage between T3 and T4; the second hydrogen bond is formed between the NH of C6 base ring and the C(O) of T1 base (Figure 10C). The bases T3, T4, and T5 of the amide-3 DNA single strand remained stacked in both "hairpin-like" conformations. In the unmodified DNA single strand, the first breakage of a base stacking was observed after 250 ps between T11 and C12. Local disorders due to the breakage of base stacking were found in a few places and no significant amount of base stacking is observed throughout the first 5 ns trajectory. The transition from a stacked conformation to an unstacked conformation was monitored using the distance between the glycosidic nitrogen atoms of two subsequent bases as a function of time.[68,69]

It was found that the *CpT dimers in the amide-3 DNA single strand have less propensity to form unstacked states compared to the corresponding pCpT in the natural DNA single strand. Amide-3 dimeric units in the DNA modified single strand showed better stacking compared to the corresponding natural DNA dimeric units, i.e., pT3*T4, T4pT5, pT7*C8, C8pT9, and C12pT13 dimers remained stacked during the first 5 ns run whereas the corresponding dimer units in the natural DNA freely rotated to the unstacked conformation. Notably, dimer units pT3*T4, T4pT5 and pT7*C8 correspond to the "hairpin-like" conformations sampled by the amide-3 DNA single strand.

(c) Structure Analysis. Furanose Ring Pucker. The effect of the amide-3 backbone modification on the pseudorotational angle profile is evidenced by comparing the pucker distribution for the amide-3 and natural DNA single strands. Figure 11 shows the histograms for the amide-3 residues *i* and residues *i* + 1 and the corresponding nucleotides in the native DNA single strand for all conformations sampled along each 10 ns simulation. In both profiles there are two distinct peaks in the distribution of the pseudorotational angles indicating that the sugar pucker in solution is free to convert from the A-form (C3′ endo) to the B-form (C2′ endo) and vice versa. For the amide-3 DNA single strand, the shape of the profiles differ from the native DNA profile indicating a different behavior of the sugar moieties.

The introduction of seven alternated amide-3 modifications led to a preference for the C3′ endo sugars at the residues i in agreement with previous experimental studies on an 8-mer amide-3 modified DNA−RNA[23] (see Figure 11A). As a reference, Figure 11B indicates the sampling of structures with mixed C2′ endo/ C3′ endo sugar puckers as expected for the natural DNA single strand.

Global and Local Flexibility of Single Strands. Monitoring of the end-to-end distance is a good indicator of the molecular global flexibility. The time evolution of the end-to-end distance was calculated by monitoring the distance between C1′ atoms of each single strand (see Figure 1). No significant difference was found in the end-to-end distance fluctuations for the natural and amide-3 DNA single strands during the dynamics (last 5 ns). The average end-to-end distances and standard deviations are 43.9 ± 8.2 and 44.7 ± 5.9 Å for the amide-3 DNA and natural DNA single strands, respectively. Calculated fluctuations were normalized by the corresponding average distances and were compared directly. It was found that the normalized fluctuation is lowest for the natural DNA (0.13) and larger for the amide-3 DNA (0.19).

The small difference found in the global dynamic behavior does not facilitate conclusions about differences in the relative global flexibility of the natural and amide-3 DNA single strands.

Features of the Single Strand Coiled States. The radius of gyration is useful to characterize the shape of the conformations adopted by the natural and amide-3 DNA single strands during the trajectories. Figure 12 shows the probability distribution of the gyration radius along the dynamics for the natural and the

(68) Norberg, J.; Nilsson, L. *Biophys. J.* **1994**, 67, 812−824.
(69) Norberg, J.; Nilsson, L. *Chem. Phys. Lett.* **1994**, *224*, 219−224.

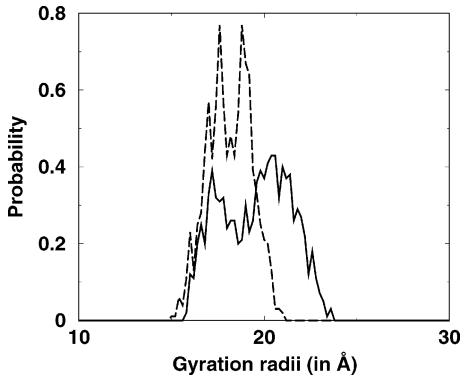

Figure 12. Probability distribution of the gyration radius along the dynamics for the unmodified (solid line) and the amide-3 (dashed line) DNA single strands.

amide-3 DNA single strands. It was found that the unmodified DNA adopts considerably extended conformations while the amide-3 DNA single strand adopts more compact coiled conformations in agreement with the conformational cluster analysis. This difference is consistent with the fact that the electrostatic repulsion between phosphate groups in the natural DNA forces the DNA to maintain an elongated conformation while the absence of such repulsion in the amide-3 DNA single strand allows the modified DNA to adopt a more globular conformation.

(d) Solvent and Counterions Structure Around Single Strands. Water Molecules. rdfs between the amide-3 atoms (i.e. O8′ and N5′ atoms in Figure 1) of the amide-3 single strand DNA and the oxygen atoms of the water molecules indicate that one ordered site occurs on the oxygen atom O8′ of each amide-3 with the position of the first peak at 2.4 Å from the oxygen atom O8′ of the carbonyl group with a degree of occupancy of 1 water molecule. In contrary, no stable sites were found in the neighborhood of NH groups of the amide-3 linkages. rdfs between the phosphorus atoms of the amide-3 DNA single strand and the oxygen atoms of the water molecules show a first peak of hydration near 3.8 Å with a coordination number of 1.5 as found for phosphorus atoms of the unmodified DNA−RNA. Thus, the presence of amide-3 linkages does not change the shell of hydration of the phosphorus atoms compared to the natural DNA single strand.

Ammonium Counterions. rdfs between the P atom (or the oxygen atoms O8′ of the amide-3 carbonyl groups) and the nitrogen of the ammonium indicate two ordered sites within the time scale of the simulation i.e., pT9 and pT11 with the first peak at 3.8 Å with a coordination number of 0.5. No ordered sites for ammonium were found coordinated to the amide-3 group.

Discussion and Conclusion

We have used a combination of experimental and theoretical techniques to study the relative binding affinities of a DNA−RNA duplex with seven alternated amide-3 linkages (3′-CH_2−CONH-5′) and the corresponding natural DNA−RNA hybrid. We performed thermal dissociation measurements of the two DNA−RNA duplexes at pH 6.0 in 10 mM NaCl/10 mM potassium phosphate buffer. The measurements indicate that the amide-3 DNA−RNA duplex with seven alternated backbone linkages is more stable (T_m = 54.2 °C ± 0.6) compared to the natural DNA−RNA (T_m = 43.6 °C ± 0.7) by about 11 °C. Analysis of thermal melting curves using the van't Hoff relationship allows the evaluation of nucleic acids stability and thereby allows evaluation of the consequence of chemical modifications on the oligomer structure. The differential melting curve can be robustly fit to only three parameters, two of which are the underlying physical constants of melting temperature (T_m) and van't Hoff enthalpy (ΔH_{vH}). van't Hoff analysis of the unmodified and amide-3 DNA−RNA hybrids shows that in the present experimental conditions, ΔH_{vH} values are −87 and −93 kcal/mol, respectively. Free energy and entropy changes corresponding to these transition enthalpies were then determined by using the Gibbs equation to calculate the corresponding terms at 298K. van't Hoff enthalpies and extrapolated ΔG values determined from the UV melting studies on the duplexes indicated that the increased thermodynamic stability of the amide-3 DNA−RNA is mainly due to an increased binding enthalpy as compared to the unmodified DNA−RNA hybrid.

Molecular dynamics simulations combined with continuum solvation methods have been used as a complementary technique for better understanding the relative binding affinity and specificity of modified and unmodified DNA single strands hybridized with a 2′-*O*-Me RNA and corresponding DNA single strands in aqueous solution at P = 1 atm and T = 300 K. We have performed 10 ns unrestrained simulations of one natural DNA−RNA duplex d(TpTpTpTpTpMpTpMpTpMpTpMpTp-MpT).2′-*O*-Me-r(CpCpCpCpCpGpCpGp CpGpCpGpCpGpC) and one DNA−RNA duplex with seven alternated amide-3 backbone linkages d(T*TpT*TpT*MpT*MpT*MpT*MpT*-MpT).2′-*O*-Me-r(CpCpCpCpCpGpCpGpCpGpCpGpCpG pC). The simulations have been carried out with explicit inclusion of solvent and counterions and with the Particle Mesh Ewald method for an accurate treatment of long-range electrostatic forces. We have used the CHARMM27 force field for nucleic acid with the addition of the amide-3 linkage topology and parameters extracted from the CHARMM22 force field for proteins. Experimental structures of the 15-mer natural and amide-3 DNA−RNA hybrids considered in the present work are not available so far. Experimental structural data on an amide-3 modified oligonucleotide reported so far relates to the investigation of conformational changes on an 8-mer amide-3 modified DNA hybridized with the complementary 2′-*O*-Me RNA hybrid.[23] The single modification which was inserted in the center of the duplex did not affect strongly the duplex structure and the sugar of residue *i* (see Figure 1) was found to adopt exclusively the C3′ endo conformation. From the present study, the replacement of seven phosphodiester linkages by seven amide-3 backbone linkages preserves a A-type conformation close to the natural DNA−RNA hybrid. While sequence-specific effects cannot be entirely ruled out, the analysis presented here, as well as other experimental[23] and theoretical studies[21] on amide-3 modified deoxyribonucleic acids, confirms that this conformational preference is driven by the amide-3 backbone linkage. Helicoidal parameters were calculated for the present MD average DNA−RNA structures and compared to the crystal structures of the DNA−RNA hybrids. The MD simulations reproduce satisfactorily the average helicoidal parameters found in the available experimental data of a polypyrimidine DNA complemented to a polypurine RNA. Despite the fact that the theoretical models of both the natural

and unmodified DNA−RNA hybrids appear to be globally in a A-form they are small differences in the DNA strands when there are compared at the local level. The average twist angle between subsequent bases indicates a global unwinding of the amide-3 DNA−RNA as compared to the natural DNA−RNA hybrid. Since the twist values between the amide-3 steps are similar to the twist values between two corresponding consecutive base pairs in the natural DNA−RNA, the global unwinding must be a consequence of a change in the twist of the steps below and above but not in the step connected by the amide-3 linkage itself. Such observations might be explained by the constrained planar (trans) conformation of the amide-3 linkage and the fact that the residues $i - 1$ and $i + 2$ have to compensate one less degree of freedom. In summary, no overall global differences between the natural and amide-3 DNA−RNA hybrids were observed as reflected in the similar RMS differences as compared to the average structures or the canonical A-form initial structures. Local differences were observed where motions of the amide-3 moieties are more flexible compared to the phosphodiester linkage also reflected by the broad distribution of the β, γ, and ϵ backbone angle values. Finally, the double strand simulations indicated that the sugar pucker amplitudes of the residues *i* are globally locked in the C3′ endo conformation whereas the natural DNA−RNA samples the C3′ endo and C2′ endo conformations. The average water structure around the unmodified and amide-3 DNA−RNA duplexes and the unmodified and amide-3 DNA single strands, characterized in this work by the radial distribution functions suggest that the amide-3 DNA−RNA hybrid duplex may have less structural water molecules sites as compared to the corresponding unmodified DNA−RNA duplex. This observation is consistent with the fact that the number of water molecules systematically linking opposite phosphate groups, which stitch the major groove of two complementary strands together and thus stabilize the natural A-form DNA−RNA duplex[18] are less in the amide-3 DNA−RNA duplex (eight vs fifteen phosphate groups).

Two additional 10 ns unrestrained molecular dynamics simulations of the natural DNA single strand d(TpTpTpTpTpMpTpMpTpMpTpMpTpMpT) and the amide-3 modified backbone DNA single strand d(T*TpT*TpT*MpT*MpT*MpT*MpT*MpT) were performed in the same conditions as the corresponding DNA−RNA double strands. For the amide-3 DNA single strand, the cluster analysis of the configurational space sampled during the first 5 ns of the simulations indicates that the most stable conformation adopted 25% of the time during the last 5 ns is characterized by a C3′ endo conformation of all T4pT5pM6pT7pM8pT9pM10pT11 sugar puckers (except M10). This result suggests that the amide-3 DNA single strand exhibits an A-type conformation in explicit water that was not observed for the natural DNA single strand in the present simulations. In addition, this result suggests that the entropic contribution to the binding of the amide-3 DNA to its complementary RNA strand is less than the corresponding natural DNA to the RNA.

The binding energies differences between the two complementary strands of the amide-3 and natural DNA−RNA hybrids were estimated using continuum solvation models combined with molecular dynamics simulations in explicit water. Changes in the solute entropy upon binding of the two complementary strands were not included in this calculation and are expected to be significant different for the amide-3 and the natural DNA single strands based on the cluster conformational analysis in explicit water. In the assessment of the calculated binding free energies, it should also be noted that changes in internal energy upon complex formation are neglected because of the use of structures from a single MD trajectory for both complementary single strands. The use of individual MD simulations for each single strand involved in the complex formation might be warranted. As a preliminary study, the two major contributors to the binding enthalpy were calculated in the present work. Charge repulsion between phosphate groups on opposite strands provides a significant unfavorable contribution to the free energy of duplex formation at physiological ionic strengths.[70,71] Thus, removal of negative charge on one strand is expected to increase duplex stability at physiological ionic strength as long as the effect of neutral charge is not offset by an unfavorable effect such as pre-organization into a structure incompatible with duplex formation. Such interactions are significantly lower in the amide-3 DNA−RNA compared to the corresponding natural duplex as seven negatively charged phosphodiester linkages have been replaced by neutral peptide-like linkages. The present preliminary thermodynamic study suggests that the more favorable binding free energy of the amide-3 DNA−RNA hybrid compared to their natural analogues might be equally due to more favorable nonpolar and electrostatic interactions between complementary strands. A complete assessment of the free energies differences from the molecular mechanical energy (E_{MM}), the solvation free energy ($G_{solvation}$), and the vibrational, rotational, and translational entropies for the DNA, following previously developed methods[48−50] is in preparation.

To the best of our knowledge, this study represents the first quantitative thermodynamic investigation of modified DNA-RNA recognition. Taken together, these observations suggest that amide-3 modified backbone DNA-RNA binding is governed by a broad range of factors, including electrostatic interactions, chemically induced structural modifications, i.e., A-form pre-organization of the amide-3 single strand in explicit water, and solvation effects without structural alterations in the host RNA. Such knowledge is required for the ultimate development of a more rational approach to drug design.

Acknowledgment. We acknowledge helpful technical support from Martin Diggelmann. R.F.-P. would like to acknowledge the assistance of M. Boehler and P. Den Hartog in the experimental work. Use of a clustering program for conformational analysis developed by M. Schaefer is gratefully acknowledged. M.N. acknowledge useful discussion with Michael Schaefer.

Supporting Information Available: Amide-3 backbone modification parameters abstracted from the CHARMM27 force field for proteins and nucleic acids and representative plots of the water radial distribution functions around the amide-3 linkage are available free of charge via Internet at http://pubs.acs.org. See any current masthead page for ordering information and Web access instructions.

JA0486566

(70) Record, M. T. Jr.; Anderson, C. F.; Lohman, T. M. *Q. Rev. Biophys.* **1978**, *11*, 103−178.
(71) Manning, G. S. *Q. Rev. Biophys.* **1978**, *11*, 179−246.